ACS OMEGA

http://pubs.acs.org/journal/acsodf

Article

# Exploring the Therapeutic Effects of Multifunctional *N*-Salicylic Acid Tryptamine Derivative against Parkinson's Disease

Xuelin Li,[§] Shuzhi Wang,[§] Shan Duan,[§] Lin Long, Linsheng Zhuo, Yan Peng, Yongxia Xiong, Shuang Li, Xue Peng, Yiguo Yan, Zhen Wang,* and Weifan Jiang*

Cite This: *ACS Omega* 2023, 8, 28910−28923

Read Online

ACCESS | Metrics & More | Article Recommendations

**ABSTRACT:** Parkinson's disease (PD) is the second most common neurodegenerative disease worldwide. Neuroinflammation and oxidative stress play an important role in the whole course of PD, which have been the focus of PD drug development. In our previous research, a series of *N*-salicylic acid tryptamine derivatives were synthesized, and the biological evaluation showed that the compound *LZWL*02003 has good anti-neuroinflammatory activity and displayed great therapeutic potency for neurodegenerative disease models. In this work, the neuroprotective efficiency of *LZWL*02003 against PD *in vitro* and *in vivo* has been explored. It was found that *LZWL*02003 could protect human neuron cells SH-SY5Y from $MPP^+$-induced neuronal damage by inhibiting ROS generation, mitochondrial dysfunction, and cellular apoptosis. Moreover, *LZWL*02003 could improve cognition, memory, learning, and athletic ability in a rotenone-induced PD rat model. In general, our study has demonstrated that *LZWL*02003 has good activity against PD in *in vitro* and *in vivo* experiments, which can potentially be developed into a therapeutic candidate for PD.

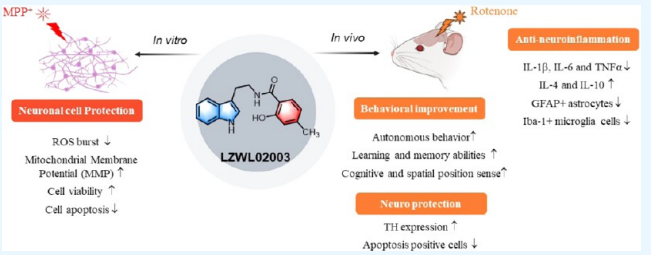


## INTRODUCTION

Neurodegenerative diseases have been the leading cause of disability in the elderly worldwide.[1] PD, the second most common neurodegenerative disease after AD, is an age-related disease, and its pathological characteristics mainly involve the absence of dopaminergic neurons and abnormal accumulation of $\alpha$-synuclein ($\alpha$-Syn) in the substantia nigra striatum of the midbrain.[2−5] The incidence of PD is ∼1 to 2% in people over 60 years old[1,6] and 3% in people over 75 years old, and it tends to increase with age.[7] Its main symptoms include resting tremors, postural gait disturbance, and bradykinesia.[4,5] In addition, PD patients are also accompanied by some nonmotor symptoms such as sleep disturbance, fatigue, anxiety, depression, and cognitive decline.[8]

The current main approach for the treatment of PD is to maintain dopamine levels. Noteworthily, these therapies only target symptom improvement and cannot prevent or delay the progression of PD. With the prolongation of medication, the efficacy will gradually weaken, and side effects such as drug-induced tremors may occur.[6,9] The increasing prevalence of PD has caused considerable difficulties in our society and economy. In view of the diverse etiology and complex pathogenesis of PD, it is urgent to develop new drugs targeting different pathogenesis to fight against PD.[10]

Many researches have shown that neuroinflammation plays a central and bridging role in the pathogenesis of PD.[11−13] Neuroinflammation can exacerbate the expression of oxidative stress, thereby exacerbating neuronal damage.[14,15] At the same time, it also can lead to excessive activation of microglial cells, which can release many harmful inflammatory factors, ultimately leading to neuronal degeneration and death.[16,17] Therefore, it is widely recognized that inhibiting neuroinflammation can be used to treat PD.[18,19]

Our previous studies have found that the *N*-salicylic acid tryptamine derivative *LZWL*02003 (Figure 1) had excellent anti-neuroinflammatory activity and exhibited great therapeutic potency for neurodegenerative disease models.[20,21] However, the therapeutic potential of *LZWL*02003 for PD is still elusive.

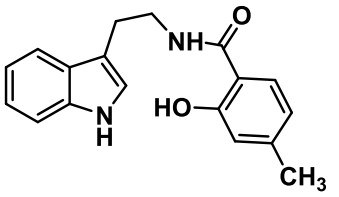


**Figure 1.** Structure of compound *LZWL*02003.

**Received:** June 15, 2023
**Accepted:** July 14, 2023
**Published:** July 28, 2023

Given this, this study conducts a systematical evaluation of anti-PD effects and the mechanism of *LZWL*02003 both *in vivo* and *in vitro* and provides a theoretical basis for PD treatment.

## MATERIALS AND METHODS

**Cell Culture.** The human neuroblastoma cell SH-SY5Y and the human microglia cell HMC3 were purchased from Procell Life Science & Technology Co., Ltd. (Wuhan, China). The SH-SY5Y cells were cultured in MEM/F12 medium supplemented with 15% FBS, 100 U/mL penicillin, and 100 U/mL streptomycin at 37 °C with 5% $CO_2$. The HMC3 cells were cultured in MEM medium supplemented with 10% FBS, 100 U/mL penicillin, and 100 U/mL streptomycin at 37 °C with 5% $CO_2$.

**Cytotoxicity Assay.** The cytotoxicity of *LZWL*02003 in SH-SY5Y and HMC3 cells was detected by the CCK8 assay according to our previous work.[20,21] In brief, 80 $\mu$L of exponentially growing cells were seeded into a 96-well plate at a density of $1 \times 10^5$ cells/mL. 20 $\mu$L of *LZWL*02003 was then added to each cell with the different final concentrations of 0, 6.25, 12.5, 25, 50, and 100 $\mu$M. After incubation at 37 °C for 24 h, 10 $\mu$L of CCK8 (Applygen, E1008, China) were added to each well. For an additional 4 h incubation at 37 °C, the cell viability was determined at 450 nm by using a microplate reader. Then, $IC_{50}$ values were determined.

**Neuron Protection Experiment.** The effect of 1-methyl-4-phenylpyridinium (ion) ($MPP^+$) (Sigma) on the survival rate of SH-SY5Y was examined. The SH-SY5Y cells were seeded into a 96-well microplate at a density of $1.0 \times 10^5$ cells/mL after digestion with 0.25% trypsin when they were in the logarithmic growth phase. The number of cells was $1.0 \times 10^4$ cells/well. 12 h later, the drug was added to the plate, and the final concentration of $MPP^+$ were 0.25, 0.5, 1, 2, and 4 mM. The cells were cultured for another 24 h after adding $MPP^+$, and the cell viability was detected by a microplate reader at a wavelength of 450 nm using the CCK8 method. According to the results, an appropriate concentration of $MPP^+$ (2 mM) was selected. And SH-SY5Y cells were seeded into the 96-well plate again. 12 h later, $MPP^+$ and compound *LZWL*02003 were added to make the final concentration of $MPP^+$ 2 mM, and the final concentrations of compound *LZWL*02003 were 5, 10, and 20 $\mu$M. After culturing for 24 h, the cell viability was detected with the microplate reader at a wavelength of 450 nm using the CCK8 method.

**Morphological Changes by Crystal Violet Staining.** The SH-SY5Y cells were seeded into a 6-well microplate at a density of $6 \times 10^5$ cells/mL after digestion with 0.25% trypsin when they were in the logarithmic growth phase. The number of cells was $1.2 \times 10^6$ cells/well. 12 h later, the drugs were added to the plate, and the final concentration of $MPP^+$ was 2 mM and the final concentrations of compound *LZWL*02003 were 5, 10, and 20 $\mu$M. Five groups were set up: control, $MPP^+$, and $MPP^+$ with low, medium, and high concentrations of *LZWL*02003. For another 24 h culturing, the culture media were removed, and 1 mL of PBS was added to each well for washing. After repeating three times, 1 mL of 4% paraformaldehyde solution (Solarbio, P1110, China) was added to each well for 5 min fixation. The cells of each well were stained with 1 mL of 0.1% crystal violet (Solarbio, G1062, China) for 5 min. Then, the stain was removed. After washing three times with PBS, the cells were observed and photographed under the microscope.

**DCFH-DA Assay Evaluation of ROS Level Changes.** The SH-SY5Y cells were seeded into a 6-well microplate at a density of $6 \times 10^5$ cells/mL after digestion with 0.25% trypsin when they were in the logarithmic growth phase. The number of cells was $1.2 \times 10^6$ cells/well. 12 h later, the drugs were added to the plate, and the final concentration of $MPP^+$ was 2 mM and the final concentrations of compound *LZWL*02003 were 5, 10 and 20 $\mu$M. Five groups were set up: control, $MPP^+$, and $MPP^+$ with low, medium, and high concentrations of *LZWL*02003. For another 24 h culturing, the culture media was removed, and 1 mL of PBS was added to each well for washing. PBS was removed, and 0.5 mL of 0.25% trypsin was added to each well for about 90 s digesting. The digestion was stopped with 2 mL of complete medium, and the cell suspensions in each well were collected with a 15 mL centrifuge tube and then centrifuged at 1500 rpm for 3 min. The culture media was removed and 1 mL of a DCFH-DA stain (prepared in 1:1000 serum-free medium as required by the kit) (Solarbio, CA1410, China) was added to each tube. The cells were incubated at 37 °C for 30 min in the dark. After washing in serum-free medium three times, the cells were resuspended in 500 $\mu$L of serum-free medium and transferred into a flow tube. All of the flow tubes were placed in a container with ice and sent to a cell flow cytometer for detection.

**Detection of the Mitochondrial Membrane Potential (MMP) by the JC-1 Assay.** The SH-SY5Y cells were seeded into a 6-well microplate at a density of $6 \times 10^5$ cells/mL after digestion with 0.25% trypsin when they were in the logarithmic growth phase. The number of cells was $1.2 \times 10^6$ cells/well. 12 h later, the drugs were added to the plate, and the final concentration of $MPP^+$ was 2 mM and the final concentrations of compound *LZWL*02003 were 5, 10, and 20 $\mu$M. Five groups were set up: control, $MPP^+$, and $MPP^+$ with low, medium, and high concentrations of *LZWL*02003. For another 24 h culturing, the culture media were removed, and 1 mL of PBS was added to each well for washing. PBS was removed, and 0.5 mL of 0.25% trypsin was added to each well for about 90 s digesting. The digestion was stopped with 2 mL of complete medium, and the cell suspensions in each well were collected with a 15 mL centrifuge tube and then centrifuged at 1500 rpm for 3 min. The culture media was removed and 1 mL of complete medium and 1 mL of JC-1 (Solarbio, M8650, China) staining working solution were added to each tube. The cells were incubated at 37 °C for 20 min in the dark. The culture media was removed, and the cells were washed with JC-1 staining buffer twice and resuspended with 500 $\mu$L of JC-1 staining buffer per tube. All of the flow tubes were placed in a container with ice and sent to the cell flow cytometer for detection.

**Assessment of Apoptosis by the Annexin V-FITC Apoptosis Detection Kit.** The SH-SY5Y cells were seeded into a 6-well microplate at a density of $6 \times 10^5$ cells/mL after digestion with 0.25% trypsin when they were in the logarithmic growth phase. The number of cells was $1.2 \times 10^6$ cells/well. 12 h later, the drugs were added to the plate, and the final concentration of $MPP^+$ was 2 mM and the final concentrations of compound *LZWL*02003 were 5, 10, and 20 $\mu$M. Five groups were set up: control, $MPP^+$, and $MPP^+$ with low, medium, and high concentrations of *LZWL*02003. For another 24 h culturing, the culture media were removed, and 1 mL of PBS was added to each well for washing. PBS was removed, and 0.5 mL of 0.25% trypsin was added to each well for about 90 s


https://doi.org/10.1021/acsomega.3c04277
ACS Omega 2023, 8, 28910−28923

digesting. The digestion was stopped with 2 mL of complete medium, and the cell suspensions in each well were collected with a 15 mL centrifuge tube and then centrifuged at 1500 rpm for 3 min. The culture media was removed and 1 mL of PBS was added to each tube for washing. After three times washing, the cells were resuspended with 100 $\mu$L of deionized water. A blank tube, a PI single-staining tube, and a FITC single-staining tube were prepared. The rest were sample tubes to be tested. The sample tubes were double-stained with PI and FITC (Solarbio, CA1020, China). After the samples were prepared, 400 $\mu$L of PBS was added to each tube. All of the flow tubes were placed in a container with ice and sent to the cell flow cytometer for detection.

**Western Blotting Assay.** Standard methods were used to perform the protein preparation and western blotting analysis. The midbrain tissues of experimental animals were taken, homogenized by a homogenizer, and then a lysate (Solarbio, R0010, China) was added and centrifuged at 4 °C at 3000 rpm for 30 min. The protein quantification was determined by the BCA protein assay kit (Applygen, P1511, China). Then, protein extracts (20 $\mu$g) were resolved in 10% SDS-PAGE (Applygen, P1027, China) and transferred to a poly(vinylidene difluoride) (PVDF) membrane (Merck Millipore, Germany). Then, TH and GAPDH (Abcam, U.K.) were incubated as primary antibodies. And finally, the enhanced chemiluminescent detection system was used for immunoblot protein detection in TH and GAPDH expression.

**Animal Experiments.** 60 male SD rats with a body weight of 180−220 g were provided by Hunan SJA Laboratory Animal Co., Ltd., which were raised in a clean-grade animal house. The rats were divided into six groups; $n$ = 10 for each group. The control group was fed normally without drug intervention. The model group was given rotenone (ROT, Sigma) 2 mg/kg/day, the Le-Dopa group was given ROT 2 mg/kg/day + Le-Dopa 20 mg/kg/day, the low-dose group was given ROT 2 mg/kg/day + *LZWL*02003 2.5 mg/kg/day, the medium-dose group was given ROT 2 mg/kg/day + *LZWL*02003 5 mg/kg/day, and the high-dose group was given ROT 2 mg/kg/day + *LZWL*02003 10 mg/kg/day. The University of South China's Experimental Animal Ethics Committee gave its approval to all of the protocols for animal research. The meals, bedding components, cages, and contact equipment utilized in the SD rats' care were all used following high-pressure disinfection in the SPF IVC animal room. The animal room was kept at a constant temperature (22 ± 2 °C), humidity (50 ± 10%), a less than 60 dB noise level, and 12 h circadian rhythm management. Following their purchase, all animals received adapted food for a week before being put to the test. Our staff has made every effort to reduce the number of animals and their suffering.

**Behavioral Tests.** *Open-Field Test.* Open-field tests can detect the spontaneous activity and exploratory behavior of rats, which is a method to evaluate autonomous behavior, exploratory behavior, and tension of experimental animals in novel environments. Rats were given 5 min to freely explore an open-field arena in order to test their levels of anxiety and inquisitive behavior. A PVC square arena measuring 900 mm ($L$) × 900 mm ($W$) × 500 mm ($H$) served as the testing apparatus, which was topped by a computer-connected video camera. Every rat was put in the arena on its own, and the rats' performances were watched. A video monitoring device automatically recorded the amount of time spent in the center and periphery of the arena as well as the distance traveled there.

*Novel Object Recognition Test.* Open-field equipment is painted white and measures 900 mm ($L$) by 900 mm ($W$) by 500 mm ($H$). Within the rectangular field, two identical objects (A, A′) were positioned at predetermined separations. The number of encounters with each object was then counted during a training session lasting 5 min with the rats in the middle of the square field. 24 h following the training session, the rats were returned to the same field, but this time one of the items (A, B) had been changed. During the test session, the rats were given full reign to explore for 5 min while the number of encounters with the original and novel object was counted. Cognitive function was measured using object cognitive ability (%), which is the ratio of contacts with the original object or the novel object over all contacts with both objects.

*Water Maze Test.* MWM testing was done in a 120 cm in diameter by 50 cm in depth circular white pool. The pool was filled to a depth of 30 cm with white nontoxic water-based nontoxic titanium dioxide, which rendered the water opaque. By adding warm water, the pool's temperature was kept at 22 ± 2 °C. The escape platform was a 33.2 $cm^2$ Plexiglas square that was positioned in the middle of the third quadrant of the pool, 17 cm away from the edge and 10 cm below the water's surface. The platform was removed from the pool for the probing test (spatial probe test), but it remained in the same location during the learning trials (place navigation test).

**Histopathological Evaluation by the H&E Staining Assay.** The obtained tissue sections underwent xylene deparaffinization before being rehydrated with ethanol solutions of varying strengths. The sections were stained for 5 min in the Harris hematoxylin solution, washed under running water, and then differentiated for 10 s in 1% hydrochloric acid ethanol. Then, tissue sections were permeabilized in xylene and dehydrated in graded ethanol. Images were taken while tissue sections were viewed using an inverted optical microscope.

**TH/DAPI Double Staining Assay.** In brief, paraffin-embedded tissue sections were deparaffinized using a standard protocol and rinsed with PBS; then, the slices were immersed in an EDTA buffer solution (pH = 9.0) and heated in an electric or microwave oven until boiling. The power was cut off, and the slices were boiled continuously for 24 min and cooled for 24 min. Then, they were taken out and cooled to room temperature. After cooling, the slices were washed with 0.01 M PBS (pH = 7.2−7.6) for 3 min and repeated 3 times. The slices were placed in a sodium borohydride solution at room temperature for 30 min and washed with tap water for 5 min. They were immersed in a 75% ethanol solution for 15 s to 1 min. Then, the slices were placed in the Sudan black dye solution at room temperature for 15 min and washed with tap water for 5 min. The slices were blocked in 10% normal serum for 60 min. For the incubation of the primary antibody, an appropriate diluted primary antibody (TH, Proteintech, 25859-1-AP, dilution rate 1:50) was added and stood still overnight at 4 °C. PBS flushing was performed for 5 min and repeated 3 times. 50−100 $\mu$L of anti-rabbit IgG-labeled fluorescent antibody drops were added, incubated at 37 °C for 60−90 min, and rinsed with PBS for 5 min and repeated 3 times. The DAPI working solution was stained at 37 °C for 10−20 min; PBS flushing was performed for 5 min and repeated 3 times. The slices were patched with buffered


https://doi.org/10.1021/acsomega.3c04277
ACS Omega 2023, 8, 28910−28923

glycerin. They were kept away from light or observed under a fluorescence microscope.

**TUNEL (FITC)/DAPI Double Staining Assay.** Section dewaxing was performed according to the same method above. For the preparation of the proteinase K working solution, the number of samples was calculated and prepared collectively, and each sample was composed of 99 μL of 1× PBS and 1 μL of 100× proteinase K. The proportion of proteinase K was used immediately. 100 μL per sample proteinase K working solution was reacted at 37 °C for 20 min; the slices were immersed and rinsed with 1× PBS three times for 5 min each time. The mixture was diluted with deionized water in a ratio of 1:5 and 100 μL per sample was added. The area of the sample was covered completely with 1× equilibration buffer for testing and then incubated at room temperature for 10−30 min. Accordingly, 34 μL of $ddH_2O$, 10 μL of 5× equilibrium buffer, 5 μL of FITC-12-dUTP labeling mix, 1 μL of recombinant terminal deoxynucleotidyl transferase (TdT) were configured with the required TdT enzyme incubation buffer (negative control system: a control incubation buffer without the TdT enzyme was prepared, and the TdT enzyme was replaced with dd $H_2O$). They were dried with absorbent paper around the balanced area using 100 μL of 1× equilibrium buffer, and then 50 μL of TdT incubation buffer was added. The cells were not allowed to dry. They were incubated at 37 °C for 60 min and light was avoided. The cells were flushed for 5 min × 3 times by PBS and light was avoided. The DAPI working solution was dyed at 37 °C for 10 min and flushed with PBS for 5 min × 3 times. Attention was paid to avoiding light. They were kept away from light or observed under a fluorescence microscope.

**Immunohistochemical Staining.** Section dewaxing was performed according to the same method above. The slices were immersed in a 0.01 M citrate buffer solution (pH = 6.0), heated in an electric or microwave oven until boiling, and then the power was cut off. The slices were boiled continuously for 20 min, cooled for 20 min, and then taken out and cooled to room temperature. Then, they were washed with 0.01 M PBS (pH = 7.2−7.6) for 3 min × 3 times. 1% periodate was added at room temperature for 10 min to inactivate endogenous enzymes. PBS flushing was performed for 3 min × 3 times. The primary antibody with proper dilution (TNF-α, IL-1β, IL-4, IL-6, and IL-10) (Abcam, U.K., dilution rate 1:200) was dripped at 4 °C overnight. PBS flushing was performed for 5 min × 3 times. 50−100 μL of the incubated anti-rabbit IgG antibody HRP polymer (Abcam, U.K.) was dripped at 37 °C for 30 min and rinsed with PBS for 5 min × 3 times. 50−100 drops of the prefabricated color-developing agent DAB working solution were added. They were incubated at room temperature for 1−5 min and washed with distilled water, and the reaction time under the microscope was controlled. Dyeing was repeated with hematoxylin for 5−10 min, they were washed with distilled water, and PBS returned to blue. Dehydration of alcohol of different levels (60−100%) was performed, 5 min for each level. They were taken out and placed in xylene for 10 min, twice, and observed with a neutral gum film and microscope.

**Immunofluorescence Detection of Glial Cell Activation Markers GFAP and Iba-1.** Section dewaxing was performed according to the same method above. The slices were then soaked in distilled water for 5 min. The slices were immersed in the EDTA buffer solution (pH = 9.0), heated in a microwave oven until boiling, and then the power was cut off. The slices were boiled continuously for 24 min, cooled for 24 min, and then taken out and cooled to room temperature. Then, they were washed with 0.01 M PBS (pH = 7.2−7.6) for 3 min × 3 times. The slices were placed in a sodium borohydride solution at room temperature for 30 min and rinsed with tap water for 5 min. Then, the slices were soaked in a 75% ethanol solution for 15 s to 1 min. The slices were placed in the Sudan black staining solution at room temperature for 15 min and rinsed with tap water for 5 min. They were sealed with 10% normal serum for 60 min. Then, appropriately diluted Glial fibrillary acidic protein (GFAP) primary antibody and ionized calcium-binding adapter molecule-1 (Iba-1) primary antibody were added (both GFAP and Iba-1 diluted at 1:50) and kept at 4 °C overnight. PBS flushing was performed for 5 min × 3 times. 50−100 μL of the anti-mouse + rabbit IgG-labeled fluorescent antibody was added dropwise, incubated at 37 °C for 60−90 min, and rinsed with PBS for 5 min × 3 times. DAPI working solution staining at 37 °C for 10−20 min and PBS flushing for 5 min × 3 times were performed. They were was sealed with buffered glycerol, stored in the dark, and observed and photos were taken under a fluorescence microscope.

**Statistical Analysis.** A minimum of three independent runs of each experiment were completed. Each sample was examined three times. The data were shown as the mean and standard deviation of the control. One-way analysis of variance (ANOVA), followed by Fisher's PLSD post hoc test for multiple comparisons, was used to establish the significance between the groups. $P < 0.05$ was regarded as statistically significant. GraphPad Prism version 9.0 (GraphPad Software, La Jolla, CA) was used for data analysis. The fluorescence statistics are computed using Image Pro Plus 6.0 software from Media Cybernetics, Silver Spring, MD.

## RESULTS

**Cytotoxicity of *LZWL*02003.** We used two cell lines, SH-SY5Y and HMC3, to detect the cytotoxicity of compound *LZWL*02003 by the CCK8 method. The results showed that the cytotoxicity of compound *LZWL*02003 was slight or negligible and suitable for further neuroactivity study (Table 1).

**Table 1. Cytotoxicity of the *LZWL*02003 (Mean ± SD)**

| cells | SH-SY5Y | HMC3 |
|---|---|---|
| $IC_{50}$ (μM) | 100.23 ± 1.28 | 228.40 ± 2.36 |

**Neuron Protection Against $MPP^+$-Induced Neuronal Damage.** $MPP^+$ was used to stimulate SH-SY5Y cells to establish a cell model of PD. As the results show in Figure 2A, when the $MPP^+$ concentration was 2 mM, the survival rate detected by the CCK8 method of SH-SY5Y was about 80%. After treatment with different concentrations (5, 10, and 20 μM) of *LZWL*02003 within 24 h, the survival rate was improved (Figure 2B). Noteworthily, when the administration time was prolonged to 48 h, the protective effect of neurons was more significant (Figure 2C). Consistent with the mentioned results above, the morphological changes of cells in the $MPP^+$ model group were sparse and the number of cells was few (Figure 2D), and in the drug intervention groups, the number of cells recovered to varying degrees and was related to the drug concentration. For detail, most of the cells in the model group were stained only by the nucleus, while the


https://doi.org/10.1021/acsomega.3c04277
ACS Omega 2023, 8, 28910−28923

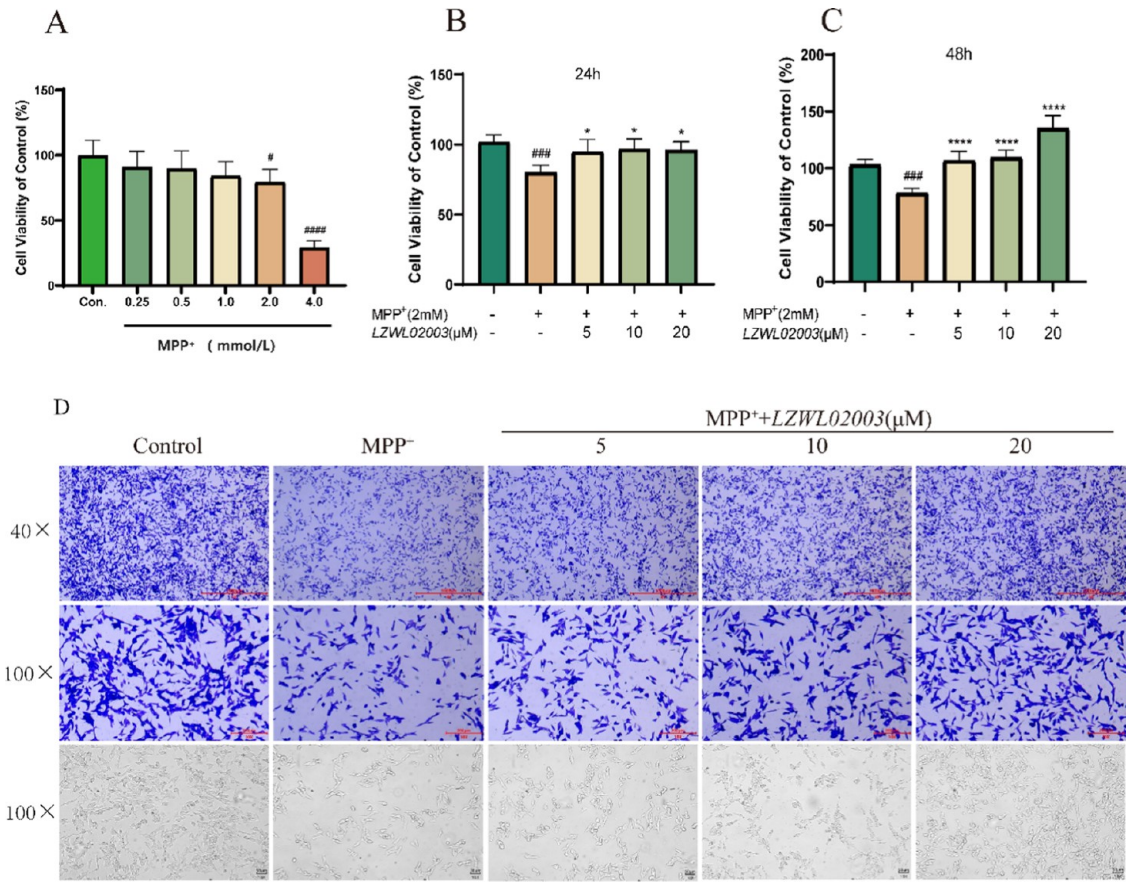


**Figure 2.** (A) Survival rate of SH-SY5Y cells was detected through the CCK8 assay after exposure to different concentrations of $MPP^+$ for 24 h. (B, C) Protection effect of *LZWL*02003 on SH-SY5Y with different concentrations (5, 10, 20 $\mu$M) after being treated with 2 mM $MPP^+$ for 24 and 48 h. (D) Slices were stained with a 1% crystal violet staining solution. Compared with the control group, the number and density of cells in the $MPP^+$ treatment group decreased, and only the cells with stained nuclei accounted for a large proportion. Compared with the $MPP^+$ group, the number and morphology of cells in each treatment group were recovered to varying degrees. Grayscale images also showed the same results. $^{\#}P < 0.05$, $^{\#\#\#}P < 0.001$, and $^{\#\#\#\#}P < 0.0001$ compared with the control group. $^{*}P < 0.05$ and $^{****}P < 0.0001$ compared with the $MPP^+$ group.

number of certain cells in the control group was fewer. The number of cells stained only by the nucleus in each intervention group was also less than that in the model group, which was preliminarily related to the concentration of the compound *LZWL*02003. The higher the concentration of *LZWL*02003, the more cells there were, and the fewer cells were stained only by the nucleus (Figure 2D). All of these results suggested that *LZWL*02003 has a clear protective effect on $MPP^+$-induced neuronal damage.

**Evaluation of the ROS Level by the DCFH-DA Assay.** Under the effect of $MPP^+$, the ROS expression in SH-SY5Y cells was significantly increased, and the difference was statistically significant compared with the model group (Figure 3A,B). After intervention with *LZWL*02003, the expression of ROS was decreased. When *LZWL*02003 was at the highest concentration (20 $\mu$M), the expression of ROS was significantly reduced compared with the model group, and the difference was statistically significant (Figure 3A,B). Thus, *LZWL*02003 could reduce the expression of ROS in the PD model of SH-SY5Y cells induced by $MPP^+$.

**Detection of MMP by the JC-1 Assay.** MMP reflects early cell apoptosis, and its decline indicates cell damage. As shown in Figure 3C, treatment with $MPP^+$ can significantly reduce the level of MMP, which can be partially restored after intervention with *LZWL*02003 in a concentration-dependent manner, and the differences were statistically significant ($P <$ 0.01). That is to say, *LZWL*02003 can increase the level of MMP and reduce the $MPP^+$-induced cell damage of SH-SY5Y cells.

**Annexin V-FITC Apoptosis Detection Kit Evaluation of Apoptosis.** Apoptosis is an important process for multicellular organisms to maintain homeostasis. The disorder of apoptosis may be directly or indirectly related to the occurrence of many diseases. The experimental results in Figure 3D,E showed that compared with the control group, the incidence of apoptosis in the model group increased significantly. After treatment with *LZWL*02003, the incidence of apoptosis was reduced. Specifically, in the high-concentration administration group, the incidence of apoptosis decreased significantly with a statistically significant difference ($P < 0.05$).

**Behavioral Tests.** An open-field experiment is a technique for assessing the autonomy, exploratory behavior, and stress of experimental animals in a novel setting. Our results of the open-field experiment showed that in terms of total distance and total time of exercise, each treatment group with *LZWL*02003 was superior to the model group, and the difference was statistically significant ($P < 0.05$). In terms of average exercise speed, there was no significant difference between the model group and the low-dose group. The middle-dose group and high-dose group of *LZWL*02003 were better than the model group, and the difference was statistically


https://doi.org/10.1021/acsomega.3c04277
ACS Omega 2023, 8, 28910−28923

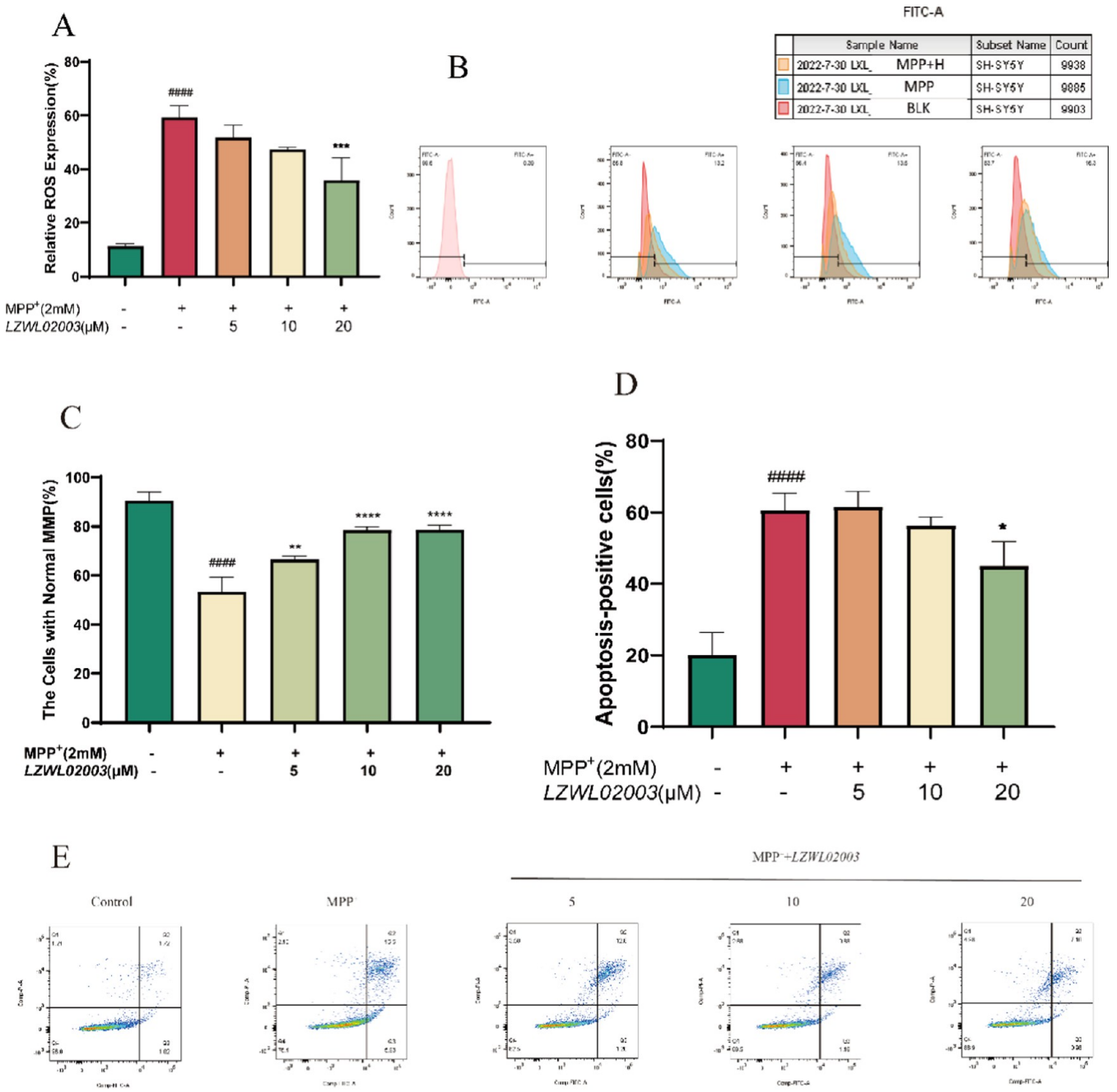


**Figure 3.** (A, B) Relative ROS expression evaluated by a cell flow meter after exposure to 2 mM $MPP^+$ for 24 h. *LZWL*02003 with different concentrations (5, 10, 20 $\mu$M) was added to treat the cells with 2 mM $MPP^+$. It can be seen that the high-dose treatment group could reduce the expression of ROS more obviously. (C) MMP results of SH-SY5Y cells. (D, E) Apoptosis-positive cells were evaluated by a cell flow meter. $^{\#\#\#\#}P < 0.0001$ compared with the control group. $^*P < 0.05$, $^{**}P < 0.01$, $^{***}P < 0.001$, and $^{****}P < 0.0001$ compared with the 2 mM $MPP^+$ treatment group.

significant ($P < 0.05$). There was no significant difference between the control group and the treatment groups with different doses of *LZWL*02003 in the above three evaluation indexes (Figure 4A–D).

The experiment of new object recognition is to evaluate the cognitive and memory abilities of animals by exploring the time of familiar objects and new strangers. The results showed that the low-dose group of *LZWL*02003 had no advantage over the model group in terms of the identification index. While the control group, the middle- and high-dose groups were better than the model group, and the difference was statistically significant ($P < 0.05$, Figure 4E). In terms of total recognition time, only the high-dose group of *LZWL*02003 had a statistical difference compared with the model group ($P < 0.05$, Figure 4F).

The water maze experiment is a test that forces experimental animals (rats) to swim and learn to find a platform hidden in the water. It is mainly used to test the learning and memory ability of experimental animals on spatial position sense and spatial positioning, as well as their motor coordination ability. The experimental results showed that the incubation period of each administration group of *LZWL*02003 was shorter than


https://doi.org/10.1021/acsomega.3c04277
ACS Omega 2023, 8, 28910−28923

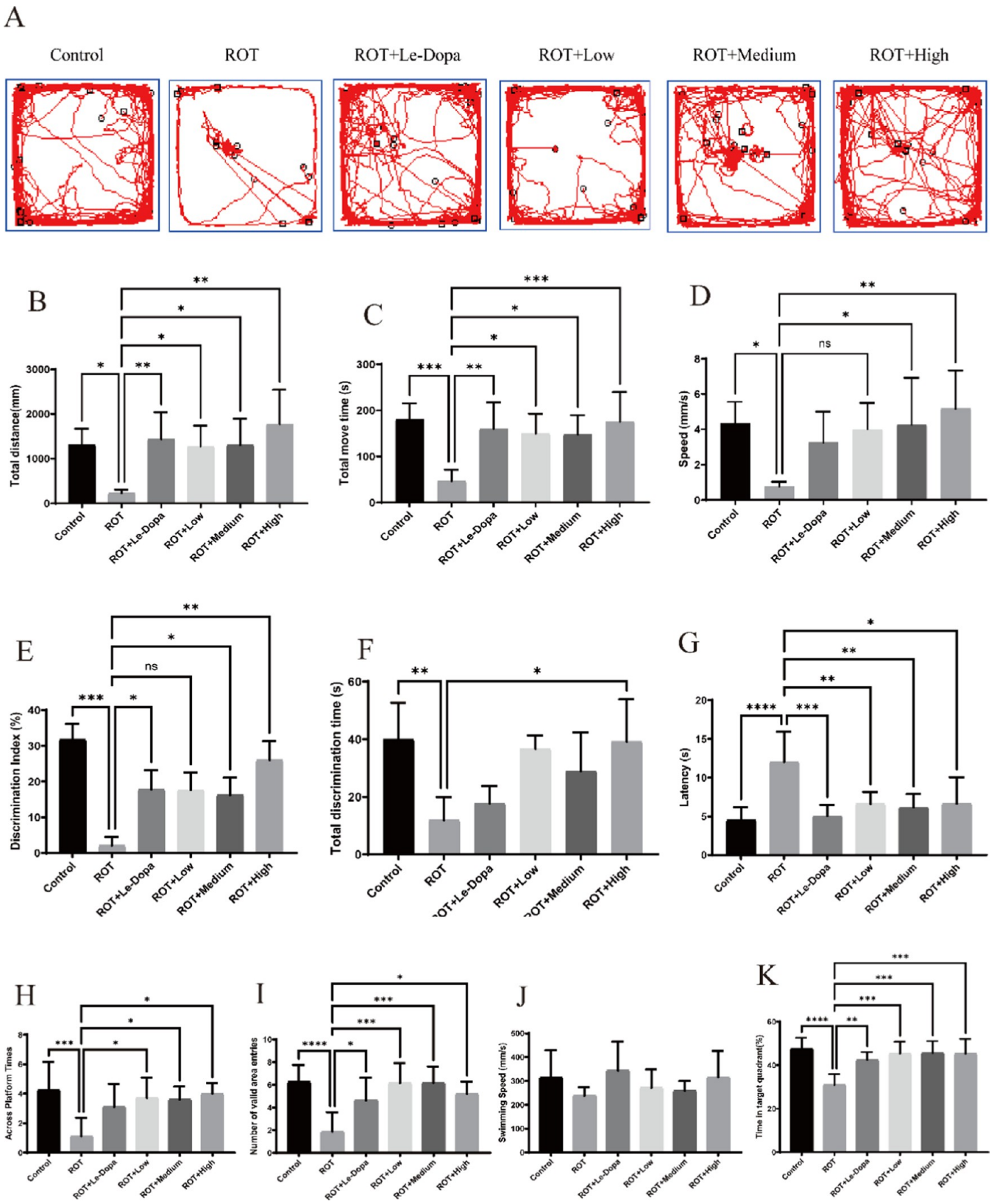


**Figure 4.** Behavior evaluation of ROT-induced PD rats. The data of the open-field experiment (A–D), new object recognition experiment (E, F), and Morris water maze test were recorded (G–K). Compared with the control or ROT group, $^{*}P < 0.05$, $^{**}P < 0.01$, $^{***}P < 0.001$, and $^{****}P < 0.0001$. Panel (D) is the average moving speed of rats in each group. Panel (J) is the average swimming speed of rats. There was no significance in swimming speed between each group. Data are mean ± SD; $n \geq 6$ animals.

that of the model group in a statistically significant difference ($P < 0.05$). Similarly, in the two statistical indicators of escape platform entry times and effective area entry times, each drug administration group of *LZWL*02003 was superior to the



https://doi.org/10.1021/acsomega.3c04277
*ACS Omega* 2023, 8, 28910−28923

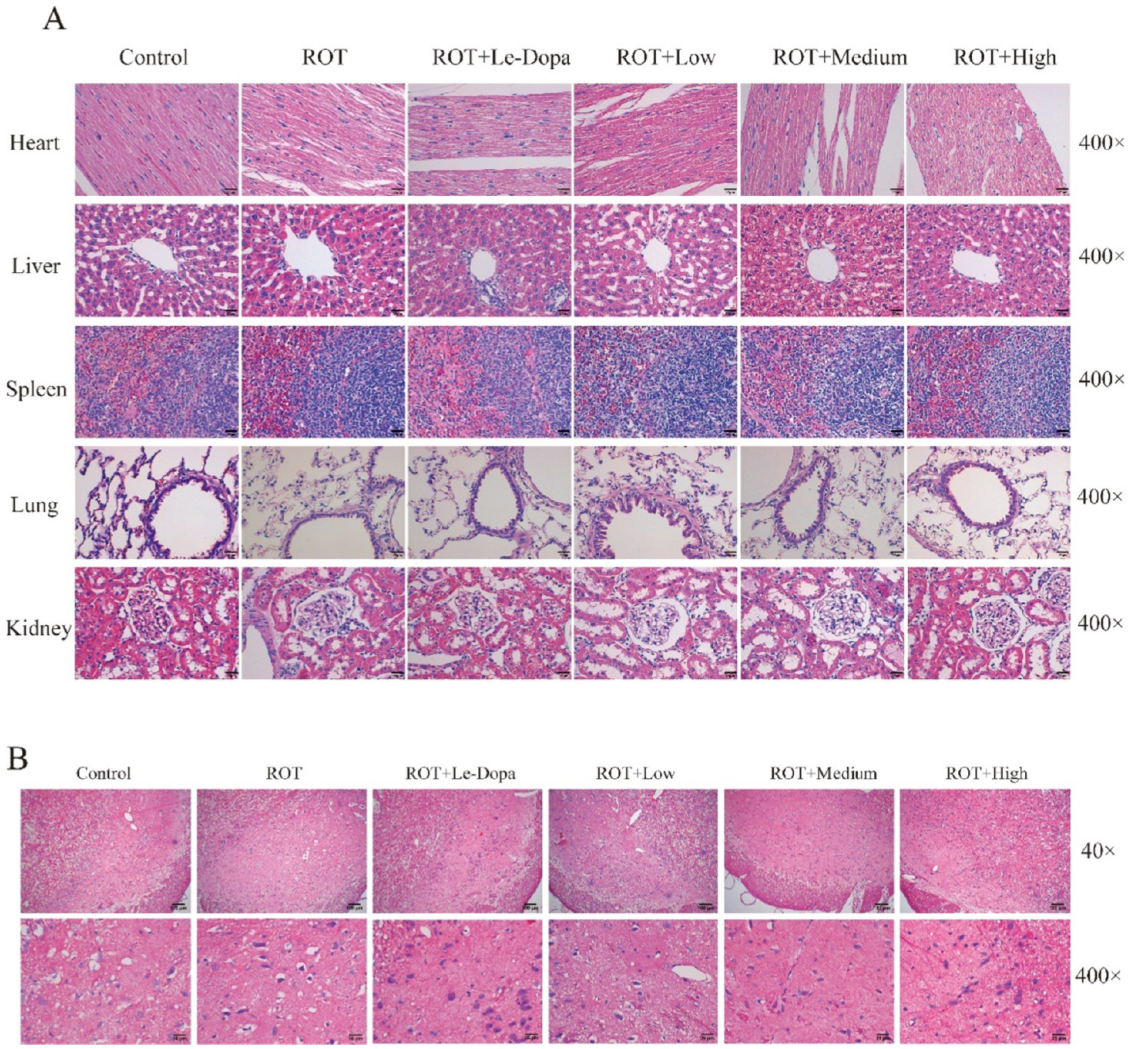


**Figure 5.** Evaluation of H&E staining sections of important organs of experimental rats. As shown in panel (A), no obvious injury or toxicity was found in the tissue sections of the heart, liver, spleen, lung, and kidney of rats. (B) H&E staining results of brain tissue sections showed that the neuronal cell death in the ROT group was more common than that in other groups, which was characterized by a small number of neurons, pyknosis of nuclei, increased vacuoles, and other signs.

model group, with a statistically significant difference ($P < 0.05$). There was no difference in average swimming speed between groups. The staying time percentage in the third quadrant of each *LZWL*02003 administration group was better than that in the model group, and the difference was statistically significant ($P < 0.05$) (Figure 4G–K).

**Histopathological Evaluation by the H&E Staining Assay.** The H&E staining assay on the tissue sections of important organs was performed to observe whether *LZWL*02003 is toxic to the animals in each group. According to the H&E staining results of heart, liver, spleen, lung, and kidney tissue sections, no signs of a toxic reaction appeared in the important organs of each group of experimental rats (Figure 5A). In addition, the H&E staining section of the midbrain tissue of rats showed that neurons in the ROT group died more commonly than the other groups (Figure 5B).

**TH/DAPI Double Staining Assay.** Tyrosine hydroxylase (TH) is an important enzyme for the production of dopamine neurotransmitters. The decrease of TH will directly lead to the decrease of dopamine neurotransmitters, which indirectly reflects the decrease of neuron cells. Therefore, the TH/DAPI double staining assay was conducted to detect the survival rate of neurons in the rat midbrain tissue. The results showed that the green fluorescence expression of TH in the ROT group was the lowest, while the expression of TH in other groups increased significantly ($P < 0.0001$) (Figure 6A–E).

**TUNEL (FITC)/DAPI Double Staining Assay.** TUNEL staining is a method used to detect the expression of apoptosis. After TUNEL double staining, the number of green fluorescence represents the number of apoptotic cell expressions. As shown in Figure 6F, the intensity of green fluorescence of neurons in the ROT group is significantly higher than that in other groups in rat midbrain tissue sections. That is, the incidence of apoptosis in the ROT group is significantly higher than that in other groups (Figure 6F).

**Immunohistochemical Staining.** In the experiment, the immunohistochemical method was used to detect the expression of various inflammatory factors including IL-1$\beta$, IL-6, IL-4, IL-10, and TNF$\alpha$ in the rat midbrain tissue. As shown in Figure 7, compared with the ROT group, the proinflammatory factors IL-1$\beta$, IL-6, and TNF$\alpha$ were decreased, and the anti-inflammatory factors IL-4 and IL-10 were increased in other groups.



https://doi.org/10.1021/acsomega.3c04277
*ACS Omega* 2023, 8, 28910−28923

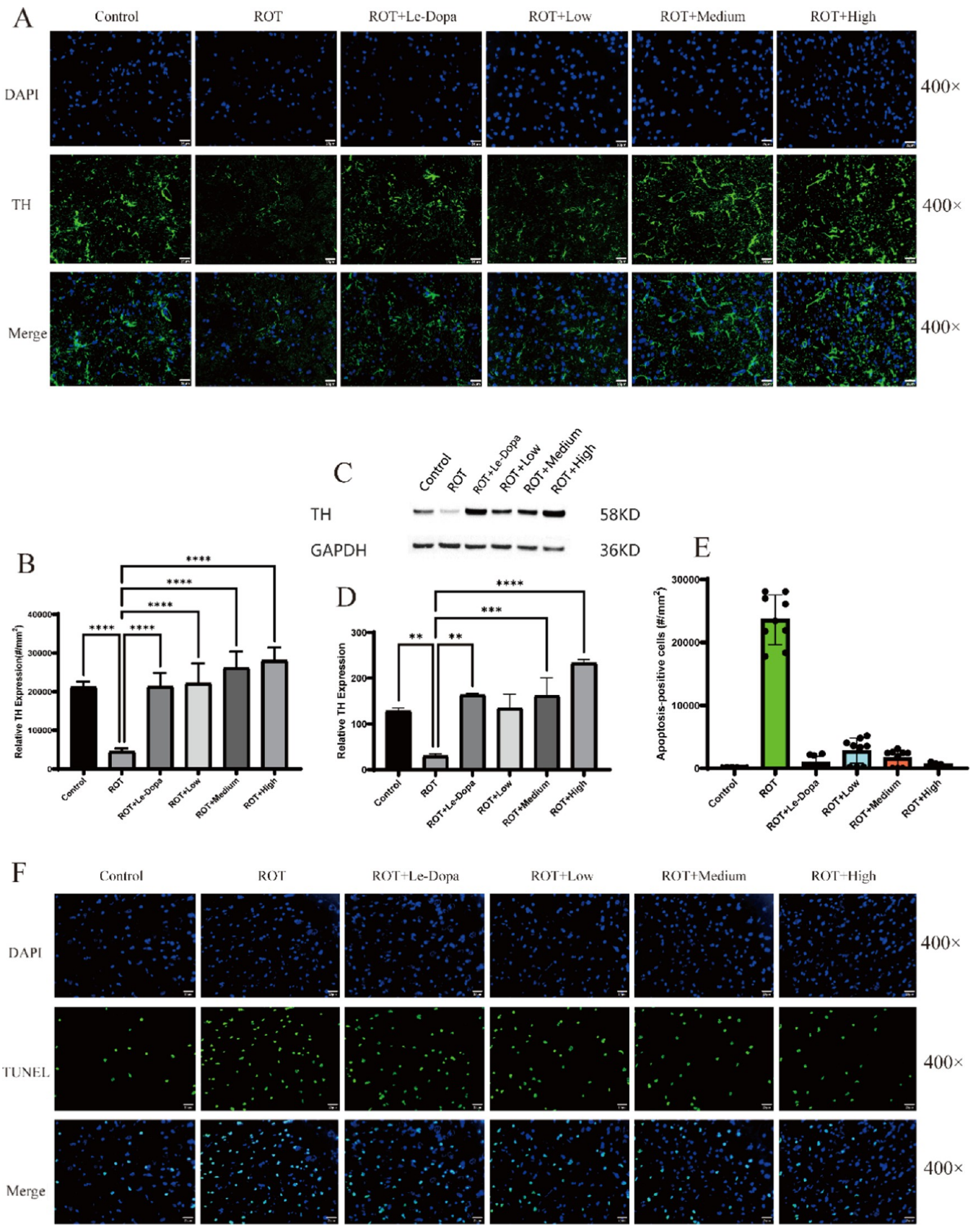


**Figure 6.** (A) Compared with the ROT group, the expression of TH in other groups increased. (B) Image Pro Plus 6.0 software is used for TH fluorescence statistics. Compared with the ROT group, the other groups had significant advantages, with statistically significant differences (****$P$ < 0.0001). (C, D) WB results showed that, compared with the ROT group, the expression of TH in rat midbrain increased with a statistically significant difference. (E, F) Compared with the ROT group, the apoptosis-positive cells were much more than other groups.



https://doi.org/10.1021/acsomega.3c04277
ACS Omega 2023, 8, 28910−28923

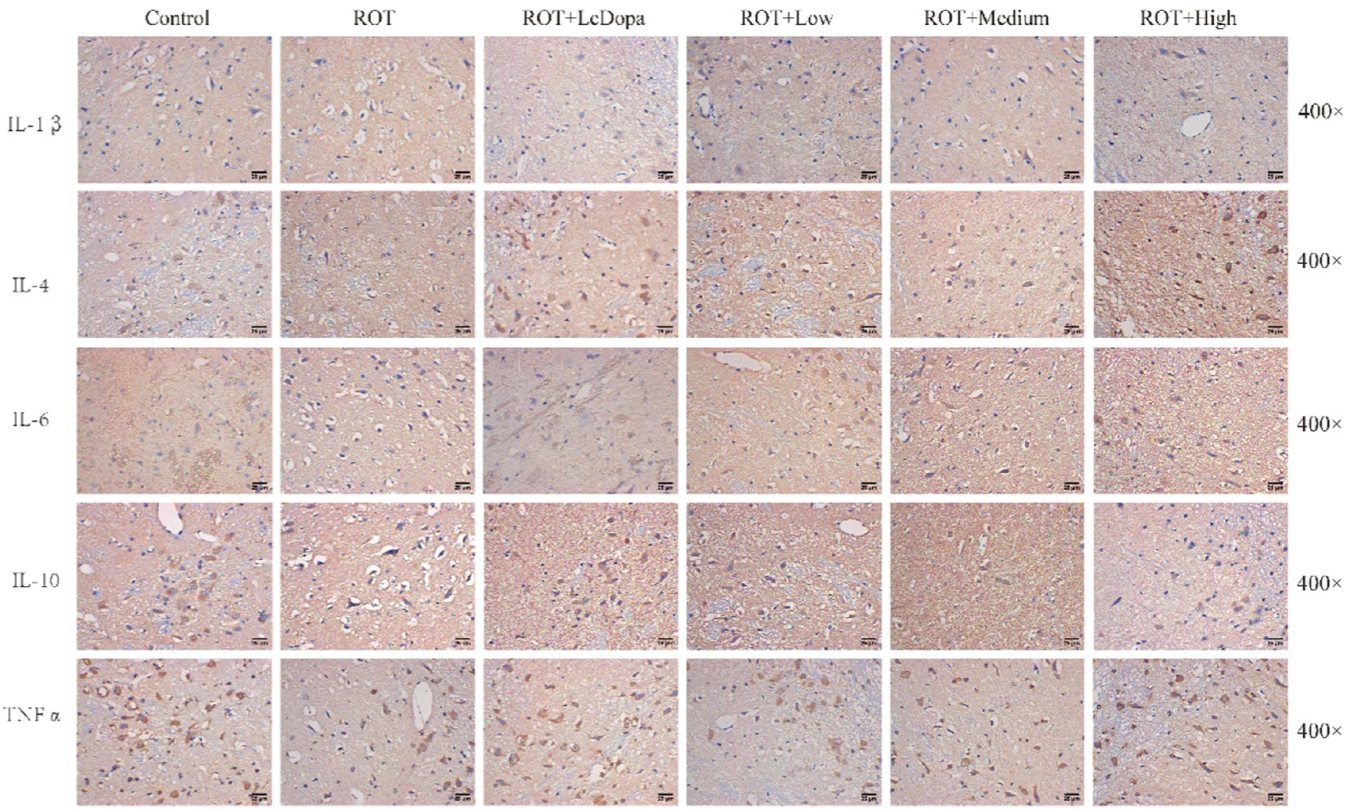


**Figure 7.** Expression of different inflammatory factors in the midbrain was detected by immunohistochemical staining. As shown here, compared with the ROT group, the expression of IL-1 $\beta$, IL-6, and TNF$\alpha$ decreased. The expression of IL-4 and IL-10 increased.

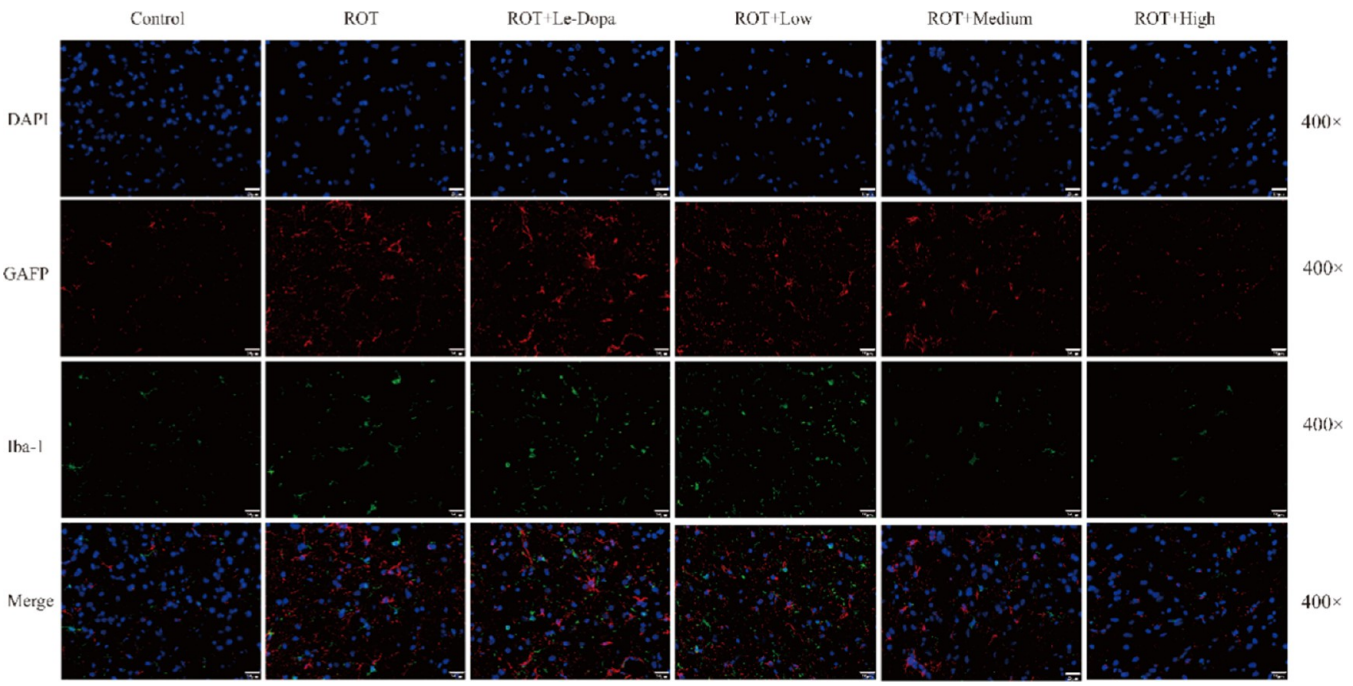


**Figure 8.** Expression of GFAP and Iba-1 in the midbrain was detected by immunohistochemical staining. Red fluorescence represents the expression of GFAP, while green fluorescence represents the expression of Iba-1. As shown here, compared with the ROT group, the expression of GFAP and Iba-1 decreased.

**Inhibitory Effects on Activation of Astrocytes and Microglial Cells.** Iba-1 was selected as a marker for the activation of microglia, and GFAP was a marker for the activation of astrocytes. The results are shown in the following figure (Figure 8) under high magnification (400×). Red fluorescence represents the expression of GFAP, while green fluorescence represents the expression of Iba-1. Compared with the ROT group, the expression levels of red and green



https://doi.org/10.1021/acsomega.3c04277
ACS Omega 2023, 8, 28910−28923

fluorescence in the control group and other treatment groups decreased, indicating a decrease in Iba-1 expression and a decrease in GFAP expression. Among them, the expression differences between the ROT + high group and the ROT group, as well as between the ROT + medium group and the ROT group, are more significant.

## DISCUSSION

PD is a common neurodegenerative disease that has been puzzling people all over the world.[22] Because of its unknown pathogenesis and complex pathological causes, the current treatment is mainly to improve the symptoms, and there is less treatment for the cause.[23−25] Considering the multiple characteristics and intricated pathogenesis of PD, developing multifunctional agents is a promising strategy to seek a breakthrough in the fundamental treatment of PD.

It is well known that the main obstacle to developing an effective drug for PD is the multifactorial and unclear pathogenesis of PD.[26] Among the extremely complex pathogeneses, neuroinflammation plays an essential role in them.[11,13,27] Neuroinflammation is a key factor in the development of PD,[28] and many studies have demonstrated that it promotes neurodegeneration and neuronal death.[29−33] Brain autopsy of PD patients revealed $CD8^+$ and $CD4^+$ T-cell infiltration and accumulation of microglia and astrocytes in the substantia nigra.[34] PET scans of the PD patients' brains showed increasing levels of neuroinflammation in regions of the pons, basal ganglia, striatum, frontal lobes, and temporal cortex, along with massive apoptosis of DA neurons.[35] Furthermore, most microglia were enriched in DA neurons in the midbrain regions.[36] Midbrain DA neurons, which are directly linked to inflammation and differ from neurons in the hippocampus or cortex, showed enhanced sensitivity to cytokines such as the tumor necrosis factor (TNF).[37,38] Generally, the persistent degeneration and death of dopaminergic neurons in the brains of PD patients is the result of neuroinflammation.[28] Given this, anti-neuroinflammatory therapy is a promising research field for combating PD.[15,39,40]

Previous studies have shown that compound *LZWL*02003 has definite anti-neuroinflammatory activity, good blood−brain barrier permeability, and low toxicity.[20] Another study showed that *LZWL*02003 had a good therapeutic effect on the mouse AD model.[21] Therefore, the cell experiment of compound *LZWL*02003 on anti-neuroinflammatory activity was not repeated in this paper, and we mainly focused on the detection of the neuroprotective effect. The persistent decrease of neurons in the substantia nigra of the midbrain in PD patients is a pathological feature of PD that leads to the decrease of dopamine neurotransmitters in the brain of PD patients[16,41] and the continuous decrease of the basic points or targets of drug treatment. Therefore, the persistent degeneration and death of neurons is a great challenge for the clinical treatment of PD. The experimental results showed that *LZWL*02003 could significantly improve the cell survival rate in the PD cell model established by $MPP^+$-induced SH-SY5Y cells, reverse the decreased MMP, reduce the incidence of apoptosis, and decrease the expression of ROS in cells. All of these observations suggested that *LZWL*02003 has a good neuroprotective effect in the PD cell model. To sum up, compound *LZWL*02003 can play a role in protecting neurons, and theoretically, it is possible to treat PD. And it is treated from the cause, not only to improve the symptoms.

In order to evaluate the possible mechanism of *LZWL*02003 on neuroprotective effects against $MPP^+$-induced cell death, the molecular mechanism of compound *LZWL*02003's anti-neuroinflammation and neuroprotective effect has been preliminarily explored. In the screening experiment of five cell death inhibitors, it was found that Nec-1 and NSA were associated with $MPP^+$-mediated SH-SY5Y cell death. When the $MPP^+$ concentration was increased to 4 mM, only Nec-1 increased the survival rate of SH-SY5Y cells. Nec-1 is a highly specific and effective necrotic apoptosis inhibitor that can penetrate the blood−brain barrier, and it is also an allosteric inhibitor of ATP competitive receptor-interacting protein kinase 1 (RIPK1).[42,43] It is a crucial upstream kinase involved in the activation of necroptosis. Necroptosis is closely related to many diseases, including inflammatory diseases and neurodegenerative diseases.[44,45] The results observed in our experiments indicate that *LZWL*02003 may play a role by interfering with the necroptosis pathway, which needs further confirmation, and relevant research is currently in progress.

In the establishment of the PD animal model, we used SD male rats by injecting ROT subcutaneously through the posterior neck of rats, which is a mature modeling method of the PD animal model.[46−50] Among many methods for establishing animal models of PD, the above method has its relative advantages: covering simple operation, strong repeatability, and good replication of clinical symptoms and pathological characteristics of PD.[51−53] In this context, we conducted systematical behavioral tests on ROT-induced PD models. The results showed that the PD symptoms of rats induced by ROT were significantly improved after treatment with different doses of *LZWL*02003. In terms of toxicity *in vivo*, no damage or toxic reaction to the important organs was observed after a 9-week administration of *LZWL*02003. The further pathological examination of midbrain tissue sections by TH staining showed that the TH fluorescence of different dosage groups was significantly stronger than that of the ROT group, indicating that the survival rate of neurons was elevated by the *LZWL*02003 administration. Consistent with this, H&E staining of the midbrain also showed that neuronal cell death in the ROT group was more common than that in other groups with *LZWL*02003, suggesting that *LZWL*02003 has a certain neuroprotective function in the rat PD model induced by ROT.

Besides, TUNEL staining results showed that compared with the ROT group, the incidence of apoptosis of brain neurons in different dosage groups of *LZWL*02003 was lower, further indicating that *LZWL*02003 can reduce the overexpression of ROT-mediated apoptosis in rat mesencephalic neurons. Moreover, the level of inflammatory factors was detected using immunohistochemical staining to further evaluate the anti-neuroinflammation efficacy *in vivo* of *LZWL*02003. The results showed that compared with the ROT group, the proinflammatory factors IL-1$\beta$, IL-6, and TNF$\alpha$ decreased in different dosage groups, and the anti-inflammatory factors IL-4 and IL-10 increased, demonstrating that *LZWL*02003 could reduce the excessive expression of harmful inflammatory factors and play a neuroprotective role.

Neuroinflammation is closely related to the activation of microglia and astrocytes.[54,55] From the results mentioned above, we know that *LZWL*02003 can reduce the overactivation of microglia and astrocytes in rat brains. And these two are the frontline of the immune response of the intracranial central nervous system, which is the initiation


https://doi.org/10.1021/acsomega.3c04277
ACS Omega 2023, 8, 28910−28923

and source of neuroinflammation.[56,57] Reducing the excessive activation of glial cells can inhibit the overexpression of neuroinflammation.[16,17] In the fluorescence staining experiment of glial cell activation markers, compared with the ROT group, the red fluorescence (GFAP) and green fluorescence (Iba-1) of each treatment group was reduced, and there was a certain concentration dependence. This means that after the intervention of *LZWL*02003, the activation marker Iba-1 of microglia and the activation marker GFAP of astrocytes in experimental rats were reduced. In view of neuroinflammation plays an important role in the etiology of PD, and the continuous degeneration and disappearance of neurons in the substantia nigra of the midbrain is a typical pathological feature of PD, compound *LZWL*02003 bearing anti-inflammatory and neuroprotective functions has a promising prospect in the treatment of PD.

## CONCLUSIONS

In conclusion, both *in vitro* and *in vivo* experiments have confirmed that compound *LZWL*02003 can play an anti-neuroinflammatory role and has a neuroprotective function. It can reduce the damage of SH-SY5Y cells induced by $MPP^+$ and also protect the midbrain neurons in the rat PD model induced by ROT. The experimental results *in vitro* and *in vivo* are consistent. Therefore, we believe that compound *LZWL*02003 has good anti-PD activity and can provide new options and theoretical support for the treatment of clinical PD. In-depth research on the mechanism of action and further optimized research are still being conducted in our laboratory.

## AUTHOR INFORMATION


### Corresponding Authors

**Zhen Wang** − *School of Pharmaceutical Science, Hengyang Medical School, University of South China, Hengyang 421001 Hunan, China; The First Affiliated Hospital, Hengyang Medical School, University of South China, Hengyang 421001 Hunan, China;* orcid.org/0000-0003-4134-1779; Phone: +86 18298311530; Email: zhenw@lzu.edu.cn

**Weifan Jiang** − *School of Pharmaceutical Science, Hengyang Medical School, University of South China, Hengyang 421001 Hunan, China*; Phone: +86 15975473615; Email: jiangwf@usc.edu.cn

### Authors

**Xuelin Li** − *School of Pharmaceutical Science, Hengyang Medical School, University of South China, Hengyang 421001 Hunan, China; The First Affiliated Hospital, Hengyang Medical School, University of South China, Hengyang 421001 Hunan, China;* orcid.org/0000-0001-8510-9387

**Shuzhi Wang** − *School of Pharmaceutical Science, Hengyang Medical School, University of South China, Hengyang 421001 Hunan, China*

**Shan Duan** − *The First Affiliated Hospital, Hengyang Medical School, University of South China, Hengyang 421001 Hunan, China*

**Lin Long** − *School of Pharmaceutical Science, Hengyang Medical School, University of South China, Hengyang 421001 Hunan, China*

**Linsheng Zhuo** − *School of Pharmaceutical Science, Hengyang Medical School, University of South China, Hengyang 421001 Hunan, China*

**Yan Peng** − *School of Pharmaceutical Science, Hengyang Medical School, University of South China, Hengyang 421001 Hunan, China*

**Yongxia Xiong** − *School of Pharmaceutical Science, Hengyang Medical School, University of South China, Hengyang 421001 Hunan, China*

**Shuang Li** − *School of Pharmaceutical Science, Hengyang Medical School, University of South China, Hengyang 421001 Hunan, China*

**Xue Peng** − *School of Pharmaceutical Science, Hengyang Medical School, University of South China, Hengyang 421001 Hunan, China*

**Yiguo Yan** − *The First Affiliated Hospital, Hengyang Medical School, University of South China, Hengyang 421001 Hunan, China*

Complete contact information is available at: https://pubs.acs.org/10.1021/acsomega.3c04277


### Author Contributions

[§]X.L., S.W., and S.D. contributed equally to this work. X.L., S.W., and S.D. are responsible for the whole project, including project design, experimental operation and analysis, and article writing; L.L., L.Z., Y.P., Y.X., S.L., and X.P. are responsible for the experimental operation, data analysis, and manuscript revision; and Y.Y., Z.W., and W.J. designed and supervised the study.

### Notes

The authors declare no competing financial interest.

## ACKNOWLEDGMENTS

This research was supported by Gansu Province Science Foundation for Distinguished Young Scholars (No. 20JR5RA304), National Natural Science Foundation of China (Nos. 22107034, 82172505), China Postdoctoral Science Foundation (2022M721544), Hunan Provincial Natural Science Foundation of China (Nos. 2022JJ40356, 2023JJ40571, 2023JJ30527).

## REFERENCES


(1) Maruthi Prasad, E.; Hung, S. Y. Behavioral Tests in Neurotoxin-Induced Animal Models of Parkinson's Disease. *Antioxidants* **2020**, *9*, No. 1007.

(2) Ascherio, A.; Schwarzschild, M. A. The epidemiology of Parkinson's disease: risk factors and prevention. *Lancet Neurol.* **2016**, *15*, 1257−1272.

(3) Mohamad, K. A.; El-Naga, R. N.; Wahdan, S. A. Neuroprotective effects of indole-3-carbinol on the rotenone rat model of Parkinson's disease: Impact of the SIRT1-AMPK signaling pathway. *Toxicol. Appl. Pharmacol.* **2022**, *435*, No. 115853.

(4) Yadav, S. K.; Rai, S. N.; Singh, S. P. Mucuna pruriens reduces inducible nitric oxide synthase expression in Parkinsonian mice model. *J. Chem. Neuroanat.* **2017**, *80*, 1−10.

(5) Rai, S. N.; Yadav, S. K.; Singh, D.; Singh, S. P. Ursolic acid attenuates oxidative stress in nigrostriatal tissue and improves neurobehavioral activity in MPTP-induced Parkinsonian mouse model. *J. Chem. Neuroanat.* **2016**, *71*, 41−49.

(6) Azmy, M. S.; Menze, E. T.; El-Naga, R. N.; Tadros, M. G. Neuroprotective Effects of Filgrastim in Rotenone-Induced Parkinson's Disease in Rats: Insights into its Anti-Inflammatory, Neurotrophic, and Antiapoptotic Effects. *Mol. Neurobiol.* **2018**, *55*, 6572−6588.

(7) Pankratz, N.; Foroud, T. Genetics of Parkinson disease. *Genet. Med.* **2007**, *9*, 801−811.

(8) Valldeoriola, F.; Salvador, A.; Gomez-Arguelles, J. M.; Marey, J.; Moya, M.; Ayuga, A.; Ramirez, F. The effects of transdermal rotigotine on non-motor symptoms of Parkinson's disease: a multicentre, observational, retrospective, post-marketing study. *Int. J. Neurosci.* **2018**, *128*, 369−375.
(9) Radhakrishnan, D. M.; Goyal, V. Parkinson's disease: A review. *Neurol. India* **2018**, *66*, 26−35.
(10) Prakash, J.; Chouhan, S.; Yadav, S. K.; Westfall, S.; Rai, S. N.; Singh, S. P. Withania somnifera alleviates parkinsonian phenotypes by inhibiting apoptotic pathways in dopaminergic neurons. *Neurochem. Res.* **2014**, *39*, 2527−2536.
(11) Ren, X.; Chen, J. F. Caffeine and Parkinson's Disease: Multiple Benefits and Emerging Mechanisms. *Front. Neurosci.* **2020**, *14*, No. 602697.
(12) Siracusa, R.; Scuto, M.; Fusco, R.; Trovato, A.; Ontario, M. L.; Crea, R.; Di Paola, R.; Cuzzocrea, S.; Calabrese, V. Anti-inflammatory and Anti-oxidant Activity of Hidrox in Rotenone-Induced Parkinson's Disease in Mice. *Antioxidants* **2020**, *9*, No. 824.
(13) Sarkar, S.; Nguyen, H. M.; Malovic, E.; Luo, J.; Langley, M.; Palanisamy, B. N.; Singh, N.; Manne, S.; Neal, M.; Gabrielle, M.; Abdalla, A.; Anantharam, P.; Rokad, D.; Panicker, N.; Singh, V.; Ay, M.; Charli, A.; Harischandra, D.; Jin, L. W.; Jin, H.; Rangaraju, S.; Anantharam, V.; Wulff, H.; Kanthasamy, A. G. Kv1.3 modulates neuroinflammation and neurodegeneration in Parkinson's disease. *J. Clin. Invest.* **2020**, *130*, 4195−4212.
(14) Ramesh, G.; MacLean, A. G.; Philipp, M. T. Cytokines and chemokines at the crossroads of neuroinflammation, neurodegeneration, and neuropathic pain. *Mediators Inflamm.* **2013**, *2013*, No. 480739.
(15) Vallée, A.; Lecarpentier, Y.; Guillevin, R.; Vallee, J. N. Circadian rhythms, Neuroinflammation and Oxidative Stress in the Story of Parkinson's Disease. *Cells* **2020**, *9*, No. 314.
(16) Kam, T. I.; Hinkle, J. T.; Dawson, T. M.; Dawson, V. L. Microglia and astrocyte dysfunction in parkinson's disease. *Neurobiol. Dis.* **2020**, *144*, No. 105028.
(17) Smajić, S.; Prada-Medina, C. A.; Landoulsi, Z.; Ghelfi, J.; Delcambre, S.; Dietrich, C.; Jarazo, J.; Henck, J.; Balachandran, S.; Pachchek, S.; Morris, C. M.; Antony, P.; Timmermann, B.; Sauer, S.; Pereira, S. L.; Schwamborn, J. C.; May, P.; Grünewald, A.; Spielmann, M. Single-cell sequencing of human midbrain reveals glial activation and a Parkinson-specific neuronal state. *Brain* **2022**, *145*, 964−978.
(18) Araújo, B.; Caridade-Silva, R.; Soares-Guedes, C.; Martins-Macedo, J.; Gomes, E. D.; Monteiro, S.; Teixeira, F. G. Neuroinflammation and Parkinson's Disease-From Neurodegeneration to Therapeutic Opportunities. *Cells* **2022**, *11*, No. 2908.
(19) Schwab, A. D.; Thurston, M. J.; Machhi, J.; Olson, K. E.; Namminga, K. L.; Gendelman, H. E.; Mosley, R. L. Immunotherapy for Parkinson's disease. *Neurobiol. Dis.* **2020**, *137*, No. 104760.
(20) Fan, X.; Li, J.; Deng, X.; Lu, Y.; Feng, Y.; Ma, S.; Wen, H.; Zhao, Q.; Tan, W.; Shi, T.; Wang, Z. Design, synthesis and bioactivity study of N-salicyloyl tryptamine derivatives as multifunctional agents for the treatment of neuroinflammation. *Eur. J. Med. Chem.* **2020**, *193*, No. 112217.
(21) Bai, Y.; Liu, D.; Zhang, H.; Wang, Y.; Wang, D.; Cai, H.; Wen, H.; Yuan, G.; An, H.; Wang, Y.; Shi, T.; Wang, Z. N-salicyloyl tryptamine derivatives as potential therapeutic agents for Alzheimer's disease with neuroprotective effects. *Bioorg. Chem.* **2021**, *115*, No. 105255.
(22) Cai, Y.; Shen, H.; Weng, H.; Wang, Y.; Cai, G.; Chen, X.; Ye, Q. Overexpression of PGC-1alpha influences the mitochondrial unfolded protein response (mtUPR) induced by MPP(+) in human SH-SY5Y neuroblastoma cells. *Sci. Rep.* **2020**, *10*, No. 10444.
(23) Liu, Y.; Geng, L.; Zhang, J.; Wang, J.; Zhang, Q.; Duan, D.; Zhang, Q. Oligo-Porphyran Ameliorates Neurobehavioral Deficits in Parkinsonian Mice by Regulating the PI3K/Akt/Bcl-2 Pathway. *Mar. Drugs* **2018**, *16*, No. 82.
(24) Liebert, A.; Bicknell, B.; Laakso, E. L.; Heller, G.; Jalilitabaei, P.; Tilley, S.; Mitrofanis, J.; Kiat, H. Improvements in clinical signs of Parkinson's disease using photobiomodulation: a prospective proof-of-concept study. *BMC Neurol.* **2021**, *21*, 256.
(25) Yedlapudi, D.; Xu, L.; Luo, D.; Marsh, G. B.; Todi, S. V.; Dutta, A. K. Targeting alpha synuclein and amyloid beta by a multifunctional, brain-penetrant dopamine D2/D3 agonist D-520: Potential therapeutic application in Parkinson's disease with dementia. *Sci. Rep.* **2019**, *9*, No. 19648.
(26) Wang, T.; Shi, C.; Luo, H.; Zheng, H.; Fan, L.; Tang, M.; Su, Y.; Yang, J.; Mao, C.; Xu, Y. Neuroinflammation in Parkinson's Disease: Triggers, Mechanisms, and Immunotherapies. *Neuroscientist* **2022**, *28*, 364−381.
(27) Siracusa, R.; Scuto, M.; Fusco, R.; Trovato, A.; Ontario, M. L.; Crea, R.; Di Paola, R.; Cuzzocrea, S.; Calabrese, V. Anti-inflammatory and Anti-oxidant Activity of Hidrox((R)) in Rotenone-Induced Parkinson's Disease in Mice. *Antioxidants* **2020**, *9*, No. 824.
(28) Rasheed, M.; Liang, J.; Wang, C.; Deng, Y.; Chen, Z. Epigenetic Regulation of Neuroinflammation in Parkinson's Disease. *Int. J. Mol. Sci.* **2021**, *22*, No. 4956.
(29) Gelders, G.; Baekelandt, V.; Van der Perren, A. Linking Neuroinflammation and Neurodegeneration in Parkinson's Disease. *J. Immunol. Res.* **2018**, *2018*, No. 4784268.
(30) Kempuraj, D.; Ahmed, M. E.; Selvakumar, G. P.; Thangavel, R.; Dhaliwal, A. S.; Dubova, I.; Mentor, S.; Premkumar, K.; Saeed, D.; Zahoor, H.; Raikwar, S. P.; Zaheer, S.; Iyer, S. S.; Zaheer, A. Brain Injury-Mediated Neuroinflammatory Response and Alzheimer's Disease. *Neuroscientist* **2020**, *26*, 134−155.
(31) Giridharan, V. V.; Reus, G. Z.; Selvaraj, S.; Scaini, G.; Barichello, T.; Quevedo, J. Maternal deprivation increases microglial activation and neuroinflammatory markers in the prefrontal cortex and hippocampus of infant rats. *J. Psychiatr. Res.* **2019**, *115*, 13−20.
(32) Lee, Y.; Lee, S.; Chang, S. C.; Lee, J. Significant roles of neuroinflammation in Parkinson's disease: therapeutic targets for PD prevention. *Arch. Pharm. Res.* **2019**, *42*, 416−425.
(33) Kong, H.; Yang, L.; He, C.; Zhou, J. W.; Li, W. Z.; Wu, W. N.; Chen, H. Q.; Yin, Y. Y. Chronic unpredictable mild stress accelerates lipopolysaccharide- induced microglia activation and damage of dopaminergic neurons in rats. *Pharmacol., Biochem. Behav.* **2019**, *179*, 142−149.
(34) McGeer, P. L.; McGeer, E. G. Glial reactions in Parkinson's disease. *Mov. Disord.* **2008**, *23*, 474−483.
(35) Gerhard, A.; Pavese, N.; Hotton, G.; Turkheimer, F.; Es, M.; Hammers, A.; Eggert, K.; Oertel, W.; Banati, R. B.; Brooks, D. J. In vivo imaging of microglial activation with [11C](R)-PK11195 PET in idiopathic Parkinson's disease. *Neurobiol. Dis.* **2006**, *21*, 404−412.
(36) Lawson, L. J.; Perry, V. H.; Dri, P.; Gordon, S. Heterogeneity in the distribution and morphology of microglia in the normal adult mouse brain. *Neuroscience* **1990**, *39*, 151−170.
(37) Block, M. L.; Zecca, L.; Hong, J. S. Microglia-mediated neurotoxicity: uncovering the molecular mechanisms. *Nat. Rev. Neurosci.* **2007**, *8*, 57−69.
(38) McGuire, S. O.; Ling, Z. D.; Lipton, J. W.; Sortwell, C. E.; Collier, T. J.; Carvey, P. M. Tumor necrosis factor alpha is toxic to embryonic mesencephalic dopamine neurons. *Exp. Neurol.* **2001**, *169*, 219−230.
(39) Singh, S. S.; Rai, S. N.; Birla, H.; Zahra, W.; Rathore, A. S.; Singh, S. P. NF-kappaB-Mediated Neuroinflammation in Parkinson's Disease and Potential Therapeutic Effect of Polyphenols. *Neurotoxic. Res.* **2020**, *37*, 491−507.
(40) Pajares, M.; Manda, G.; Bosca, L.; Cuadrado, A.; et al. Inflammation in Parkinson's Disease: Mechanisms and Therapeutic Implications. *Cells* **2020**, *9*, No. 1687.
(41) Piao, Y. S.; Lian, T. H.; Hu, Y.; Zuo, L. J.; Guo, P.; Yu, S. Y.; Liu, L.; Jin, Z.; Zhao, H.; Li, L. X.; Yu, Q. J.; Wang, R. D.; Chen, S. D.; Chan, P.; Wang, X. M.; Zhang, W. Restless legs syndrome in Parkinson disease: Clinical characteristics, abnormal iron metabolism and altered neurotransmitters. *Sci. Rep.* **2017**, *7*, No. 10547.
(42) Cao, L.; Mu, W. Necrostatin-1 and necroptosis inhibition: Pathophysiology and therapeutic implications. *Pharmacol. Res.* **2021**, *163*, No. 105297.


https://doi.org/10.1021/acsomega.3c04277
*ACS Omega* 2023, 8, 28910−28923

(43) Chen, L.; Zhang, X.; Ou, Y.; Liu, M.; Yu, D.; Song, Z.; Niu, L.; Zhang, L.; Shi, J. Advances in RIPK1 kinase inhibitors. *Front. Pharmacol.* **2022**, *13*, No. 976435.
(44) Chaouhan, H. S.; Vinod, C.; Mahapatra, N.; Yu, S. H.; Wang, I. K.; Chen, K. B.; Yu, T. M.; Li, C. Y. Necroptosis: A Pathogenic Negotiator in Human Diseases. *Int. J. Mol. Sci.* **2022**, *23*, No. 12714.
(45) Zhang, S.; Tang, M. B.; Luo, H. Y.; Shi, C. H.; Xu, Y. M. Necroptosis in neurodegenerative diseases: a potential therapeutic target. *Cell Death Dis.* **2017**, *8*, No. e2905.
(46) Lin, Q.; Hou, S.; Dai, Y.; Jiang, N.; Lin, Y. Monascin exhibits neuroprotective effects in rotenone model of Parkinson's disease via antioxidation and anti-neuroinflammation. *NeuroReport* **2020**, *31*, 637−643.
(47) Javed, H.; Meeran, M. F. N.; Azimullah, S.; Bader Eddin, L.; Dwivedi, V. D.; Jha, N. K.; Ojha, S. alpha-Bisabolol, a Dietary Bioactive Phytochemical Attenuates Dopaminergic Neurodegeneration through Modulation of Oxidative Stress, Neuroinflammation and Apoptosis in Rotenone-Induced Rat Model of Parkinson's disease. *Biomolecules* **2020**, *10*, No. 1421.
(48) Chen, L.; Huang, Y.; Yu, X.; Lu, J.; Jia, W.; Song, J.; Liu, L.; Wang, Y.; Huang, Y.; Xie, J.; Li, M. Corynoxine Protects Dopaminergic Neurons Through Inducing Autophagy and Diminishing Neuroinflammation in Rotenone-Induced Animal Models of Parkinson's Disease. *Front. Pharmacol.* **2021**, *12*, No. 642900.
(49) Jayaraj, R. L.; Beiram, R.; Azimullah, S.; Meeran, M. F. N.; Ojha, S. K.; Adem, A.; Jalal, F. Y. Lycopodium Attenuates Loss of Dopaminergic Neurons by Suppressing Oxidative Stress and Neuroinflammation in a Rat Model of Parkinson's Disease. *Molecules* **2019**, *24*, No. 2182.
(50) Ostendorf, F.; Metzdorf, J.; Gold, R.; Haghikia, A.; Tonges, L. Propionic Acid and Fasudil as Treatment Against Rotenone Toxicity in an In Vitro Model of Parkinson's Disease. *Molecules* **2020**, *25*, No. 2502.
(51) Miyazaki, I.; Asanuma, M. The Rotenone Models Reproducing Central and Peripheral Features of Parkinson's Disease. *NeuroSci* **2020**, *1*, 1−14.
(52) Chia, S. J.; Tan, E. K.; Chao, Y. X. Historical Perspective: Models of Parkinson's Disease. *Int. J. Mol. Sci.* **2020**, *21*, No. 2464.
(53) Rai, S. N.; Singh, P. Advancement in the modelling and therapeutics of Parkinson's disease. *J. Chem. Neuroanat.* **2020**, *104*, No. 101752.
(54) Henry, V.; Paillé, V.; Lelan, F.; Brachet, P.; Damier, P. Kinetics of microglial activation and degeneration of dopamine-containing neurons in a rat model of Parkinson disease induced by 6-hydroxydopamine. *J. Neuropathol. Exp. Neurol.* **2009**, *68*, 1092−1102.
(55) Zhou, H.; Liu, Z.; Liu, J.; Wang, J.; Zhou, D.; Zhao, Z.; Xiao, S.; Tao, E.; Suo, W. Z. Fractionated radiation-induced acute encephalopathy in a young rat model: cognitive dysfunction and histologic findings. *Am. J. Neuroradiol.* **2011**, *32*, 1795−1800.
(56) Weiss, F.; Labrador-Garrido, A.; Dzamko, N.; Halliday, G. Immune responses in the Parkinson's disease brain. *Neurobiol. Dis.* **2022**, *168*, No. 105700.
(57) Singh, D. Astrocytic and microglial cells as the modulators of neuroinflammation in Alzheimer's disease. *J. Neuroinflamm.* **2022**, *19*, 206.

## NOTE ADDED IN PROOF

The animal study was reviewed and approved by the Medical Animal Experiment Center of the University of South China.


https://doi.org/10.1021/acsomega.3c04277
*ACS Omega* 2023, 8, 28910−28923